

Cite as: C. Dacon *et al.*, *Science* 10.1126/science.abq3773 (2022).

Broadly neutralizing antibodies target the coronavirus fusion peptide

Cherrelle Dacon^{1†}, Courtney Tucker^{1†}, Linghang Peng^{2†}, Chang-Chun D. Lee^{3†}, Ting-Hui Lin³, Meng Yuan³, Yu Cong⁴, Lingshu Wang⁵, Lauren Purser¹, Jazmean K. Williams⁶, Chul-Woo Pyo⁷, Ivan Kosik⁸, Zhe Hu⁸, Ming Zhao⁹, Divya Mohan¹, Andrew J. R. Cooper¹, Mary Peterson¹⁰, Jeff Skinner¹⁰, Saurabh Dixit⁴, Erin Kollins⁴, Louis Huzella⁴, Donna Perry⁴, Russell Byrum⁴, Sanae Lembirik⁴, David Drawbaugh⁴, Brett Eaton⁴, Yi Zhang⁵, Eun Sung Yang⁵, Man Chen⁵, Kwanyee Leung⁵, Rona S. Weinberg¹¹, Amarendra Pegu⁵, Daniel E. Geraghty⁷, Edgar Davidson⁶, Iyadh Douagi¹², Susan Moir¹³, Jonathan W. Yewdell⁸, Connie Schmaljohn⁴, Peter D. Crompton¹⁰, Michael R. Holbrook⁴, David Nemazee², John R. Mascola⁵, Ian A. Wilson^{3,14}, Joshua Tan^{1*}

¹Antibody Biology Unit, Laboratory of Immunogenetics, National Institute of Allergy and Infectious Diseases, National Institutes of Health, Rockville, MD 20852, USA.

²Department of Immunology and Microbiology, The Scripps Research Institute, La Jolla, CA 92037, USA. ³Department of Integrative Structural and Computational Biology, Scripps Research Institute, La Jolla, CA 92037, USA. ⁴Integrated Research Facility, Division of Clinical Research, National Institute of Allergy and Infectious Diseases, National Institutes of Health, Frederick, MD 21702, USA. ⁵Vaccine Research Center, National Institute of Allergy and Infectious Diseases, National Institutes of Health, Bethesda, MD 20892, USA. ⁶Integral Molecular, Philadelphia, PA 19104, USA. ⁷Clinical Research Division, Fred Hutchinson Cancer Research Center, Seattle, WA 98109, USA. ⁸Cellular Biology Section, Laboratory of Viral Diseases, National Institute of Allergy and Infectious Diseases, National Institutes of Health, Bethesda, MD 20892, USA. ⁹Protein Chemistry Section, Research Technologies Branch, National Institute of Allergy and Infectious Diseases, National Institutes of Health, Rockville, MD 20852, USA. ¹⁰Malaria Infection Biology and Immunity Section, Laboratory of Immunogenetics, National Institute of Allergy and Infectious Diseases, National Institutes of Health, Rockville, MD 20852, USA. ¹¹New York Blood Center, Lindsley F. Kimball Research Institute, New York, NY 10065, USA. ¹²Flow Cytometry Section, Research Technologies Branch, National Institute of Allergy and Infectious Diseases, National Institutes of Health, Bethesda, MD 20892, USA. ¹³B Cell Immunology Section, Laboratory of Immunoregulation, National Institute of Allergy and Infectious Diseases, National Institutes of Health, Bethesda, MD 20892, USA. ¹⁴The Skaggs Institute for Chemical Biology, The Scripps Research Institute, La Jolla, CA, 92037, USA.

[†]These authors contributed equally to this work.
*Corresponding author. Email: tanj4@nih.gov

The potential for future coronavirus outbreaks highlights the need to broadly target this group of pathogens. We use an epitope-agnostic approach to identify six monoclonal antibodies that bind to spike proteins from all seven human-infecting coronaviruses. All six antibodies target the conserved fusion peptide region adjacent to the S2' cleavage site. COV44-62 and COV44-79 broadly neutralize alpha and beta coronaviruses, including SARS-CoV-2 Omicron subvariants BA.2 and BA.4/5, albeit with lower potency than RBD-specific antibodies. In crystal structures of Fabs COV44-62 and COV44-79 with the SARS-CoV-2 fusion peptide, the fusion peptide epitope adopts a helical structure and includes the arginine at the S2' cleavage site. COV44-79 limited disease caused by SARS-CoV-2 in a Syrian hamster model. These findings highlight the fusion peptide as a candidate epitope for next-generation coronavirus vaccine development.

Coronaviruses consist of four genera of viruses that infect birds and mammals (1). Seven coronaviruses are known to cause human disease: the alphacoronaviruses HCoV-229E and HCoV-NL63, as well as the betacoronaviruses HCoV-OC43, HCoV-HKU1, SARS-CoV, MERS-CoV and SARS-CoV-2. While the first four coronaviruses generally cause mild disease, the latter three have caused serious outbreaks in recent years. In particular, the ongoing coronavirus disease 2019 (COVID-19) pandemic by SARS-CoV-2 has resulted in more than six million deaths since the first cases were identified in 2019 (2). The currently dominant SARS-CoV-2 Omicron BA.2, BA.2.12.1 and BA.4/BA.5 subvariants are at least partially resistant to most available vaccines and antibody therapeutics (3–6). Furthermore, two coronaviruses previously linked only to animal infection were recently detected in individuals with flu-like symptoms (7, 8). These developments highlight the

importance of targeting conserved and functionally essential sites on coronaviruses.

Coronavirus infection is a multi-step process that involves enzymatic cleavage and rearrangement of the surface spike protein (9). The SARS-CoV-2 spike contains two cleavage sites: a furin cleavage site at the boundary of the S1 and S2 subunits, and an S2' site that is conserved in all coronaviruses. The spike protein is thought to be cleaved at the S1/S2 site during virus assembly, leaving the S1 and S2 subunits non-covalently linked. During entry, the SARS-CoV-2 spike protein uses the receptor-binding domain (RBD) on the S1 subunit to engage angiotensin-converting enzyme-2 (ACE2) on target cells. Following receptor binding, the S1 subunit is shed and the S2' site is cleaved by the membrane enzyme transmembrane serine protease 2 (TMPRSS2) or endosomal cathepsins (7), leading to the insertion of the fusion peptide into the cell membrane and viral fusion.

Much of the protection provided by COVID-19 vaccines arises from neutralizing antibodies that target the RBD (10). Likewise, all currently available therapeutic monoclonal antibodies (mAbs) target this domain (3). However, spike elements that participate in the subsequent stages of infection involve the more complex S2 fusion machinery with many moving parts and these elements are more conserved than the RBD, which so far has been capable of retaining or even increasing binding to ACE2 despite a variety of mutations (11). Therefore, these sites are worth exploring as targets for novel COVID-19 vaccines and therapeutics that retain efficacy against new variants and protect against a wider range of coronaviruses. Progress in this direction has started with recent studies identifying several mAbs that target the conserved stem helix (12–16) and using unbiased approaches to screen for mAbs of interest (17–20). Here we undertake a large-scale survey of the binding landscape of broadly reactive mAbs against coronaviruses.

Identification of broadly reactive mAbs from COVID-19 convalescent donors

To identify individuals likely to harbor B cells that produce broadly reactive mAbs, we used a multiplex bead-based assay to examine plasma samples of 142 donors from a previously described cohort of COVID-19 convalescent individuals (20). We assessed plasma immunoglobulin G (IgG) reactivity toward spike glycoproteins of the seven human coronaviruses: SARS-CoV-2 (Wuhan Hu-1), SARS-CoV-1, MERS-CoV, HCoV-HKU1, HCoV-OC43, HCoV-NL63 and HCoV-229E. Nineteen donors were selected for mAb isolation and characterization based on plasma IgG reactivity to the spike proteins of SARS-CoV-2 and at least two other betacoronaviruses (fig. S1A).

We next interrogated human IgG⁺ memory B cells (MBCs) from the selected donors using a two-stage screen to prioritize isolating mAbs with the greatest possible breadth of reactivity. First, we screened supernatants from 673,671 stimulated IgG⁺ B cells for binding to the coronavirus spike panel used in the plasma screen. Supernatants from only 2% ($n = 211$) of the MBC culture wells met our criteria for broad reactivity by binding at least three betacoronavirus spike proteins (Fig. 1A). Next, we developed an optofluidics assay to isolate individual MBCs of interest using the Berkeley Lights Beacon system (fig. S1B). Candidate MBCs identified in the supernatant screen were sorted individually into nanoliter-volume pens and assessed in real-time for secretion of mAbs that bound to beads coated with a cocktail of MERS-CoV and HCoV-OC43 spikes, followed by beads coated with SARS-CoV-2 spike. Double positive MBCs were exported for single-cell reverse transcription-PCR (RT-PCR) and antibody production as recombinant IgG1. In total, we obtained 60 IgG mAbs with reactivity to at least three coronaviruses.

To fully interrogate their breadth, we tested the 60 mAbs for binding to spikes from the seven human coronaviruses. Only six mAbs, COV91-27, COV44-62, COV44-79, COV77-04, COV77-39 and COV78-36, bound to spike proteins from all seven coronaviruses (Fig. 1, B and C). Notably, four of the six also bound to spike from two new coronaviruses recently associated with human disease: Canine CoV HuPn-2018 (CCoV-HuPn-2018) and Porcine Deltacoronavirus 0081-4 (PDCoV-0081-4) (7, 8) (Fig. 1C). The six broadly reactive mAbs were isolated from four different donors and were encoded by four different heavy chain variable (VH) genes (VH1-2, VH3-30, VH4-59, VH5-10-1) (table S1). Five mAbs were highly mutated, with VH nucleotide mutation frequencies ranging from 10 to 13% (fig. S1C). Given that these mAbs were isolated from COVID-19 convalescent individuals in New York approximately one month after the first outbreak in March 2020, these mutation levels suggest that the B cells were primed during an earlier seasonal coronavirus infection and possibly reactivated during SARS-CoV-2 infection.

COV44-62 and COV44-79 broadly neutralize coronaviruses

We assessed the neutralizing potency of the six mAbs against SARS-CoV-2, SARS-CoV-1, MERS-CoV, HCoV-NL63 and HCoV-229E envelope pseudotyped viruses, as well as authentic HCoV-OC43. COV44-62 and COV44-79 showed the broadest functional reactivity, neutralizing the betacoronaviruses SARS-CoV-2, SARS-CoV-1 and HCoV-OC43, as well as the alphacoronavirus HCoV-NL63 and HCoV-229E (Fig. 1D and fig. S1D). Moreover, both mAbs neutralized SARS-CoV-2 variants of concern, including the Omicron BA.2 and BA.4/5 subvariants, as well as authentic SARS-CoV-2 (Fig. 1E and fig. S1E). COV44-62 also neutralized MERS-CoV, whereas no other mAbs neutralized this virus within the concentrations tested.

Broadly reactive mAbs target the coronavirus fusion peptide

To determine the domain of SARS-CoV-2 spike that was targeted by the six broadly reactive mAbs, we assessed mAb binding to the SARS-CoV-2 S2 subunit, as well as the RBD and N-terminal domain (NTD) of the S1 subunit. All six mAbs bound only to the S2 subunit (Fig. 2A). VJ germline-reverted versions of the broadly neutralizing mAbs COV44-62 and COV44-79 showed weaker binding to S2 than the mutated versions (fig. S2A), suggesting that somatic mutations were important for improving binding to the target site. A surface plasmon resonance (SPR) kinetics assay determined the binding affinity of antigen-binding fragments (Fabs) derived from these mAbs for pre-fusion stabilized whole SARS-CoV-2 spike (2P, with an intact S1/S2 cleavage site) and the unmodified S2 subunit. The Fabs bound with low-to-moderate nanomolar affinity to both proteins, but their affinity for the S2 subunit

was 3- to 76-fold higher than their affinity for whole spike (Fig. 2B and fig. S2A). There were no substantial differences between the six Fabs in their affinity for the S2 subunit. The mAbs showed reduced binding to a form of S2 that had been stabilized with two proline mutations (S2-2P) and bound more poorly still to a further stabilized version with six proline mutations (S2-HexaPro) (Fig. 2C). SPR-based competition showed that the six mAbs competed for the same binding site on the S2 subunit (Fig. 2D), but none competed with S2P6, a control mAb targeting the stem helix region (12), indicating their specificity for a distinct site on S2.

To further interrogate the specificity of these mAbs, we performed SPR-based peptide mapping using an array of 15-mer overlapping peptides that spanned the entire SARS-CoV-2 S2 subunit (Ser686 to Lys1211, Accession #YP_009724390.1). All six mAbs bound to peptides 42-44, which share the $s_{15}RSFIEDLLF_{823}$ motif (Fig. 3A). This motif is located within the SARS-CoV-2 fusion peptide region, directly C-terminal to the S2' cleavage site. To determine the diversity of this region across coronaviruses, we selected 34 viral isolates representing each of the coronavirus genera – *alpha*, *beta*, *gamma*, and *delta* (Fig. 3B). Each amino-acid position in the $s_{15}RSFIEDLLF_{823}$ motif was conserved in >90% of all viruses selected except F_{817} , which was conserved in <50% of isolates examined (Fig. 3, B and C). The fusion peptide appears partially surface-exposed in a range of coronavirus spike proteins, including SARS-CoV-2, SARS-CoV, MERS-CoV and MHV (21, 22) (Fig. 3C and fig. S3A). However, antibody access to this site may be partially occluded by the S1 subunit on an adjacent protomer, consistent with their stronger binding to the S2 subunit relative to SARS-CoV-2 spike (Fig. 2B and fig. S3B).

That these mAbs target the fusion peptide is consistent with their reduced binding to the HexaPro S2 construct (Fig. 2C), which includes a non-conservative F817P mutation at this site (23). To identify critical amino acids for mAb binding, we performed an alanine scan on a peptide encompassing residues 810 to 830 and focused on residues targeted by the broadly neutralizing mAbs COV44-62 and COV44-79 (Fig. 3D). Four amino acids, E819, D820, L822 and F823, were important for binding of COV44-62, where mutation of the F823 residue abolished binding. Similarly, critical residues for the binding of COV44-79 were E819, D820 and F823, but also included R815 at the S2' cleavage site (Fig. 3D). All five residues identified as important for COV44-62 or COV44-79 binding are among the most conserved residues in the coronavirus spike protein. D820 and L822 are completely conserved, while R815, E819 and F823 are conserved in 34 out of 35 coronaviruses (Fig. 3, B and E). Amino-acid mutations at the peptide level may have different effects from mutations in the intact spike protein, where modified interactions with surrounding residues may also affect antibody binding.

Therefore, we screened the six mAbs using a shotgun alanine mutagenesis approach, whereby every amino acid in the S2 subunit of intact spike was individually mutated to generate a panel of spike mutants (Fig. 3F and fig. S3, C and D). In general, this assay identified a greater number of residues as important for mAb binding, including some with a more intermediate phenotype. For COV44-62, D820, L822 and F823 were again crucial for binding, while K825 and D830, as well as R815, were also identified as important (Fig. 3F). For COV44-79, the results closely matched the peptide alanine scan, with the same four amino acids, R815, E819, D820 and F823, identified as the most critical. When the six mAbs were analyzed as a group, we found that only the four broadest neutralizing mAbs were negatively affected by the R815A mutation (fig. S4, A and B), suggesting that binding to the S2' cleavage site may be a distinguishing property of broadly neutralizing mAbs against this site.

Crystal structures of anti-fusion peptide antibodies

To elucidate the molecular characteristics of anti-fusion peptide antibodies that neutralize SARS-CoV-2, the Fabs of the three broadest neutralizing mAbs COV44-62, COV44-79, and COV91-27 were complexed with 15-mer peptides containing the fusion peptide sequence (Fig. 4). Crystal structures were determined to 1.46 Å, 2.8 Å and 2.3 Å resolution, respectively (Fig. 4, fig. S5 and table S2). Fourteen of the 15 peptide residues were visible in the electron density map for COV44-62 (fig. S5A), 13 of which have a buried surface area (BSA) >0 Å² in complex with antibody. For COV44-79, 12 of the 15 peptide residues were visible (fig. S5A), 10 of which have a buried surface >0 Å². Similarly, in COV91-27, 12 peptide residues had interpretable density (Fig. 4C and fig. S5A), with nine exhibiting a buried surface >0 Å². The fusion peptide forms a helix as in the prefusion state of the SARS-CoV-2 spike (fig. S5B). All three complementarity-determining regions (CDRs) of the heavy chain (HC) of all three Fabs are involved in peptide recognition whereas CDR1 and CDR3 of the light chain (LC) of COV44-62 and only LCDR3 of COV44-79 and COV91-27 contact the peptide (Fig. 4, A to C). The BSA on each Fab is dominated by the heavy chain and is 791 Å² for COV44-62 (627 Å² by HC and 164 Å² by LC), 573 Å² for COV44-79 (505 Å² by HC and 129 Å² by LC), and 573 Å² for COV91-27 (447 Å² by HC and 126 Å² by LC). The fusion peptide makes side-chain and backbone H-bonds and salt bridges with COV44-62 mainly through K814, R815, E819, D820, L822, F823 and N824, and hydrophobic interactions through I818, L822, and F823 (Fig. 4D). These residues include the key residues, E819, D820, L822 and F823 identified by site-directed mutagenesis (Fig. 3D). The fusion peptide did not form as many interactions with COV44-79 and COV91-27 (Fig. 4, E and F). However, R815, E819, and D820 contributed H-bonds and salt bridges, and I818, L822, and F823 made hydrophobic

interactions. In all three antibodies, R815, S816, I818, E819, D820, L822, and F823 contributed the most buried surface area to the interaction (Fig. 4, G to I). There was partial overlap between the residues of COV44-62 and COV44-79 that interacted with the fusion peptide and those that were mutated from germline (fig. S6), consistent with the reduction in binding of germline-reverted versions of these mAbs (fig. S2A). The structural results are consistent with the mutagenesis data with peptide and spike protein that identify the key binding residues (Fig. 3, D to F, and fig. S3D). Importantly, the arginine at the S2' cleavage site is involved in recognition by these anti-fusion peptide antibodies. Although the antibodies all interact with one face of the fusion peptide helical structure (fig. S5D), their approach angles to the peptide differ. Superimposition of the fusion peptide structures onto an intact SARS-CoV-2 spike trimer structure in the pre-fusion state showed a potential clash with the S protein, suggesting that a conformational change or conformational dynamics around the fusion peptide is required to accommodate antibody targeting (fig. S5C). Notwithstanding, these antibodies have neutralization activity against SARS-CoV-2 and therefore are able to interact with the fusion peptide on the virus (Fig. 1D).

Response to the fusion peptide following vaccination and infection

We compared the binding of polyclonal IgG from mRNA-1273-vaccinated donors (fig. S7A), COVID-19 convalescent individuals, and COVID-19-naïve individuals to the SARS-CoV-2 fusion peptide (peptide 43) (Fig. 3A and fig. S7B). All COVID-19-naïve donors showed minimal binding to the peptide, indicating a minor contribution by previous seasonal coronavirus infections to circulating fusion peptide-specific IgG. While there was an increased response in several vaccinees after the 2nd vaccine dose ($P = 0.025$), this was not enhanced by the administration of a booster. The COVID-19 convalescent donors did not have significantly higher responses than vaccinated donors ($P = 0.864$ versus post-2nd dose). However, several convalescent donors had the highest responses in all three cohorts, suggesting that SARS-CoV-2 infection triggers a strong fusion peptide-specific antibody response in some individuals.

COV44-62 and COV44-79 inhibit membrane fusion

Spike-mediated cell fusion relies on insertion of the fusion peptide into the target cell membrane and thus might be inhibited by antibody binding to the fusion peptide. Consistent with this, COV44-62 and COV44-79 inhibited the fusion of cells expressing SARS-CoV-2 spike and cells expressing the ACE2 receptor in an imaging-based assay (Fig. 5A). We further tested the six fusion peptide-specific mAbs in a more quantitative assay wherein fusion would trigger the release

of an enzyme that cleaves a chromogenic substrate. Only the mAbs that neutralized SARS-CoV-2 were able to strongly inhibit fusion (Fig. 5B).

COV44-79 limits disease in the Syrian hamster model

We evaluated the in vivo efficacy of COV44-62 and COV44-79 against SARS-CoV-2 infection in the Syrian hamster model, a well-established model recapitulating features of moderate to severe COVID-19 in humans (24–26). We converted the Fc regions of the two mAbs to hamster IgG2 to allow optimal Fc function. The mAbs were administered intraperitoneally at 16 mg/kg, followed by intranasal administration of 5 log₁₀ PFU of SARS-CoV-2 WA01 24 hours later (Fig. 5, C and D, and fig. S8). Hamsters treated with COV44-79, and to a lesser extent COV44-62, had a smaller decrease in body weight and recovered more quickly than untreated hamsters ($P < 0.01$ from days 3–7 for COV44-79 and $P < 0.05$ from days 5–7 for COV44-62) (Fig. 5C). Similar results were observed in a second experiment where COV44-79 was tested in comparison to a hamster IgG2 isotype control (fig. S7B). Furthermore, semi-quantitative scoring revealed that hamsters treated with COV44-79 had less interstitial pneumonia than untreated hamsters on day 7 ($P < 0.05$) (Fig. 5D). COV44-79 was also able to slightly reduce lung viral titers relative to control hamsters based on sub-genomic RNA quantification and plaque assay analysis (fig. S8C).

Discussion

The broad conservation and functional importance of the fusion peptide highlight the potential of this site as a candidate for coronavirus vaccine development. These findings have parallels to work done on HIV-1 gp120, where the surface-exposed fusion peptide was identified as a target of neutralizing mAbs (27). This discovery led to the investigation of the HIV-1 fusion peptide as a candidate immunogen to elicit broadly neutralizing antibodies in animals (28); subsequent animal studies have increased the potency and breadth of the fusion peptide-targeting antibody response (29). Despite these potential advantages, the coronavirus fusion peptide has not been a major focus for development of therapeutic mAbs and COVID-19 vaccines. The main drawback of the mAbs described here is their comparatively low in vitro neutralization potency. These mAbs fit into a wider trend of a trade-off between potency and breadth: highly potent mAbs targeting the RBD are restricted to sarbecoviruses and most do not neutralize all variants of SARS-CoV-2 (3, 5, 6, 20, 30), while mAbs targeting the stem helix (12–16) and those identified here have greater breadth but are less potent. However, as previously reported for at least one anti-stem helix mAb (15), COV44-79 performed better in the hamster model than expected, suggesting that it may function in a way that is not captured effectively in the neutralization assay. For instance,

Fc effector functions may enhance activity, as observed with anti-SARS-CoV-2 antibodies with other specificities (31–33). Moreover, there is substantial scope for improvement for mAbs with this specificity and subsequent studies may discover mAbs with higher potency, as with the HIV-1 fusion peptide (34). Techniques to improve antibody affinity and potency could also be useful (35, 36).

Additionally, vaccination with fusion peptide constructs may trigger a polyclonal response of greater magnitude and potency. We found that three doses of the mRNA-1273 vaccine did not produce strong antibody responses to the fusion peptide although several COVID-19 convalescent individuals had strong antibody responses to this site. This observation is consistent with greater exposure of the S2 subunit to B cells during natural infection due to S1 uncoupling, which likely occurs less frequently with pre-fusion stabilized spike protein. Furthermore, depletion of fusion peptide-specific antibodies from the serum of COVID-19 convalescent patients resulted in a 20% reduction in SARS-CoV-2 neutralization (37), and reactivity to the fusion peptide correlated with neutralization titer (38), indicating that polyclonal antibodies to the fusion peptide can play an appreciable role. Thus, our findings are consistent with previous studies highlighting the potential utility of the fusion peptide as a target epitope (37–40) and the fusion peptide-targeted mAbs provide additional tools to combat COVID-19 and enhance pandemic preparedness.

REFERENCES AND NOTES

- P. V'kovski, A. Kratzel, S. Steiner, H. Stalder, V. Thiel, Coronavirus biology and replication: Implications for SARS-CoV-2. *Nat. Rev. Microbiol.* **19**, 155–170 (2021). [doi:10.1038/s41579-020-00468-6](https://doi.org/10.1038/s41579-020-00468-6) Medline
- E. Dong, H. Du, L. Gardner, An interactive web-based dashboard to track COVID-19 in real time. *Lancet Infect. Dis.* **20**, 533–534 (2020). [doi:10.1016/S1473-3099\(20\)30120-1](https://doi.org/10.1016/S1473-3099(20)30120-1) Medline
- S. Iketani, L. Liu, Y. Guo, L. Liu, J. F.-W. Chan, Y. Huang, M. Wang, Y. Luo, J. Yu, H. Chu, K.-K.-H. Chik, T. T.-T. Yuen, M. T. Yin, M. E. Sobieszczky, Y. Huang, K.-Y. Yuen, H. H. Wang, Z. Sheng, D. D. Ho, Antibody evasion properties of SARS-CoV-2 Omicron sublineages. *Nature* **604**, 553–556 (2022). [doi:10.1038/s41586-022-04594-4](https://doi.org/10.1038/s41586-022-04594-4) Medline
- N. Andrews, J. Stowe, F. Kirsebom, S. Toffa, T. Rickard, E. Gallagher, C. Gower, M. Kall, N. Groves, A.-M. O'Connell, D. Simons, P. B. Blomquist, A. Zaidi, S. Nash, N. Iwani Binti Abdul Aziz, S. Thelwall, G. Dabreria, R. Myers, G. Amirthalingam, S. Gharbia, J. C. Barrett, R. Elson, S. N. Ladhan, N. Ferguson, M. Zambon, C. N. J. Campbell, K. Brown, S. Hopkins, M. Chand, M. Ramsay, J. Lopez Bernal, Covid-19 vaccine effectiveness against the Omicron (B.1.1.529) variant. *N. Engl. J. Med.* **386**, 1532–1546 (2022). [doi:10.1056/NEJMoa2119451](https://doi.org/10.1056/NEJMoa2119451) Medline
- E. Takashita, N. Kinoshita, S. Yamayoshi, Y. Sakai-Tagawa, S. Fujisaki, M. Ito, K. Iwatsuki-Horimoto, S. Chiba, P. Halfmann, H. Nagai, M. Saito, E. Adachi, D. Sullivan, A. Pekosz, S. Watanabe, K. Maeda, M. Imai, H. Yotsuyanagi, H. Mitsuya, N. Ohmagari, M. Takeda, H. Hasegawa, Y. Kawaoka, Efficacy of antibodies and antiviral drugs against Covid-19 Omicron variant. *N. Engl. J. Med.* **386**, 995–998 (2022). [doi:10.1056/NEJMcp2119407](https://doi.org/10.1056/NEJMcp2119407) Medline
- A. VanBlargan, J. M. Errico, P. J. Halfmann, S. J. Zost, J. E. Crowe Jr., L. A. Purcell, Y. Kawaoka, D. Corti, D. H. Fremont, M. S. Diamond, An infectious SARS-CoV-2 B.1.1.529 Omicron virus escapes neutralization by therapeutic monoclonal antibodies. *Nat. Med.* **28**, 490–495 (2022). [doi:10.1038/s41591-021-01678-y](https://doi.org/10.1038/s41591-021-01678-y) Medline
- J. A. Lednicky, M. S. Tagliamonte, S. K. White, M. A. Elbadry, M. M. Alam, C. J. Stephenson, T. S. Bonny, J. C. Loeb, T. Telisma, S. Chavannes, D. A. Ostrov, C. Mavian, V. M. Beau De Rochars, M. Salemi, J. G. Morris Jr., Independent infections of porcine deltacoronavirus among Haitian children. *Nature* **600**, 133–137 (2021). [doi:10.1038/s41586-021-04111-z](https://doi.org/10.1038/s41586-021-04111-z) Medline
- A. N. Vlasova, A. Diaz, D. Damtie, L. Xiu, T.-H. Toh, J. S.-Y. Lee, L. J. Saif, G. C. Gray, Novel canine coronavirus isolated from a hospitalized patient with pneumonia in East Malaysia. *Clin. Infect. Dis.* **74**, 446–454 (2022). [doi:10.1093/cid/ciab456](https://doi.org/10.1093/cid/ciab456) Medline
- C. B. Jackson, M. Farzan, B. Chen, H. Choe, Mechanisms of SARS-CoV-2 entry into cells. *Nat. Rev. Mol. Cell Biol.* **23**, 3–20 (2022). [doi:10.1038/s41580-021-00418-x](https://doi.org/10.1038/s41580-021-00418-x) Medline
- J. S. Tregoning, K. E. Flight, S. L. Higham, Z. Wang, B. F. Pierce, Progress of the COVID-19 vaccine effort: Viruses, vaccines and variants versus efficacy, effectiveness and escape. *Nat. Rev. Immunol.* **21**, 626–636 (2021). [doi:10.1038/s41577-021-00592-1](https://doi.org/10.1038/s41577-021-00592-1) Medline
- T. N. Starr, A. J. Greaney, S. K. Hilton, D. Ellis, K. H. D. Crawford, A. S. Dingens, M. J. Navarro, J. E. Bowen, M. A. Tortorici, A. C. Walls, N. P. King, D. Veesler, J. D. Bloom, Deep mutational scanning of SARS-CoV-2 receptor binding domain reveals constraints on folding and ACE2 binding. *Cell* **182**, 1295–1310.e20 (2020). [doi:10.1016/j.cell.2020.08.012](https://doi.org/10.1016/j.cell.2020.08.012) Medline
- D. Pinto, M. M. Sauer, N. Czudnochowski, J. S. Low, M. A. Tortorici, M. P. Housley, J. Noack, A. C. Walls, J. E. Bowen, B. Guarino, L. E. Rosen, J. di Iulio, J. Jerak, H. Kaiser, S. Islam, S. Jaconi, N. Sprugasci, K. Culap, R. Abdelnabi, C. Foo, L. Coelmont, I. Bartha, S. Bianchi, C. Silacci-Fregnii, J. Bassi, R. Marzi, E. Vetti, A. Cassotta, A. Ceschi, P. Ferrari, P. E. Cippà, O. Giannini, S. Ceruti, C. Garzonì, A. Riva, F. Benigni, E. Cameroni, L. Piccoli, M. S. Pizzuto, M. Smithey, D. Hong, A. Telenti, F. A. Lempp, J. Neyts, C. Havenar-Daughton, A. Lanzavecchia, F. Sallusto, G. Snell, H. W. Virgin, M. Beltramello, D. Corti, D. Veesler, Broad betacoronavirus neutralization by a stem helix-specific human antibody. *Science* **373**, 1109–1116 (2021). [doi:10.1126/science.abj3321](https://doi.org/10.1126/science.abj3321) Medline
- M. M. Sauer, M. A. Tortorici, Y.-J. Park, A. C. Walls, L. Hornad, O. J. Acton, J. E. Bowen, C. Wang, X. Xiong, W. de van der Schueren, J. Quispe, B. G. Hoffstrom, B.-J. Bosch, A. T. McGuire, D. Veesler, Structural basis for broad coronavirus neutralization. *Nat. Struct. Mol. Biol.* **28**, 478–486 (2021). [doi:10.1038/s41594-021-00596-4](https://doi.org/10.1038/s41594-021-00596-4) Medline
- C. Wang, R. van Haperen, J. Gutiérrez-Álvarez, W. Li, N. M. A. Okba, I. Albulessu, I. Widjaja, B. van Dieren, R. Fernandez-Delgado, I. Sola, D. L. Hurdiss, O. Daramola, F. Grosfeld, F. J. M. van Kuppeveld, B. L. Haagmans, L. Enjuanes, D. Drabek, B.-J. Bosch, A conserved immunogenic and vulnerable site on the coronavirus spike protein delineated by cross-reactive monoclonal antibodies. *Nat. Commun.* **12**, 1715 (2021). [doi:10.1038/s41467-021-21968-w](https://doi.org/10.1038/s41467-021-21968-w) Medline
- P. Zhou, M. Yuan, G. Song, N. Beutler, N. Shaabani, D. Huang, W. T. He, X. Zhu, S. Callaghan, P. Yong, F. Anzanello, L. Peng, J. Ricketts, M. Parren, E. Garcia, S. A. Rawlings, D. M. Smith, D. Nemazee, J. R. Teijaro, T. F. Rogers, I. A. Wilson, D. R. Burton, R. Andrabí, A human antibody reveals a conserved site on betacoronavirus spike proteins and confers protection against SARS-CoV-2 infection. *Sci. Transl. Med.* **14**, eabi9215 (2022). [doi:10.1126/scitranslmed.abi9215](https://doi.org/10.1126/scitranslmed.abi9215) Medline
- W. Li, Y. Chen, J. Prévost, I. Ullah, M. Lu, S. Y. Gong, A. Tauzin, R. Gasser, D. Vézina, S. P. Anand, G. Goyette, D. Chaterjee, S. Ding, W. D. Tolbert, M. W. Grunst, Y. Bo, S. Zhang, J. Richard, F. Zhou, R. K. Huang, L. Esser, A. Zeher, M. Côté, P. Kumar, J. Sodroski, D. Xia, P. D. Uchil, M. Pazgier, A. Finzi, W. Mothes, Structural basis and mode of action for two broadly neutralizing antibodies against SARS-CoV-2 emerging variants of concern. *Cell Rep.* **38**, 110210 (2022). [doi:10.1016/j.celrep.2021.110210](https://doi.org/10.1016/j.celrep.2021.110210) Medline
- F. Amanat, M. Thapa, T. Lei, S. M. S. Ahmed, D. C. Adelsberg, J. M. Carreño, S. Strohmeier, A. J. Schmitz, S. Zafar, J. Q. Zhou, W. Rijnink, H. Alshammary, N. Borchering, A. G. Reiche, K. Srivastava, E. M. Sordillo, H. van Bakel, J. S. Turner, G. Bajic, V. Simon, A. H. Ellebedy, F. Krammer, Personalized Virology Initiative, SARS-CoV-2 mRNA vaccination induces functionally diverse antibodies to NTD, RBD, and S2. *Cell* **184**, 3936–3948.e10 (2021). [doi:10.1016/j.cell.2021.06.005](https://doi.org/10.1016/j.cell.2021.06.005) Medline
- K. A. Huang, T. K. Tan, T.-H. Chen, C.-G. Huang, R. Harvey, S. Hussain, C.-P. Chen, A. Harding, J. Gilbert-Jaramillo, X. Liu, M. Knight, L. Schimanski, S.-R. Shih, Y.-C. Lin, C.-Y. Cheng, S.-H. Cheng, Y.-C. Huang, T.-Y. Lin, J.-T. Jan, C. Ma, W. James, R. S. Daniels, J. W. McCauley, P. Rijal, A. R. Townsend, Breadth and function of

- antibody response to acute SARS-CoV-2 infection in humans. *PLOS Pathog.* **17**, e1009352 (2021). [doi:10.1371/journal.ppat.1009352](https://doi.org/10.1371/journal.ppat.1009352) Medline
19. W. N. Voss, Y. J. Hou, N. V. Johnson, G. Delidakis, J. E. Kim, K. Javanmardi, A. P. Horton, F. Bartzoka, C. J. Paresi, Y. Tanno, C.-W. Chou, S. A. Abbasi, W. Pickens, K. George, D. R. Boutz, D. M. Towers, J. R. McDaniel, D. Billick, J. Goike, L. Rowe, D. Batra, J. Pohl, J. Lee, S. Gangappa, S. Sambhara, M. Gadush, N. Wang, M. D. Person, B. L. Iverson, J. D. Gollinar, J. M. Dye, A. S. Herbert, I. J. Finkelstein, R. S. Baric, J. S. McLellan, G. Georgiou, J. J. Lavinder, G. C. Ippolito, Prevalent, protective, and convergent IgG recognition of SARS-CoV-2 non-RBD spike epitopes. *Science* **372**, 1108–1112 (2021). [doi:10.1126/science.abg5268](https://doi.org/10.1126/science.abg5268) Medline
 20. H. Cho, K. K. Gonzales-Wartz, D. Huang, M. Yuan, M. Peterson, J. Liang, N. Beutler, J. L. Torres, Y. Cong, E. Postnikova, S. Bangaru, C. A. Talana, W. Shi, E. S. Yang, Y. Zhang, K. Leung, L. Wang, L. Peng, J. Skinner, S. Li, N. C. Wu, H. Liu, C. Dacon, T. Moyer, M. Cohen, M. Zhao, F. E.-H. Lee, R. S. Weinberg, I. Douagi, R. Gross, C. Schmaljohn, A. Pegu, J. R. Mascola, M. Holbrook, D. Nemazee, T. F. Rogers, A. B. Ward, I. A. Wilson, P. D. Crompton, J. Tan, Bispecific antibodies targeting distinct regions of the spike protein potently neutralize SARS-CoV-2 variants of concern. *Sci. Transl. Med.* **13**, eabj5413 (2021). [doi:10.1126/scitranslmed.abj5413](https://doi.org/10.1126/scitranslmed.abj5413) Medline
 21. A. C. Walls, M. A. Tortorici, B.-J. Bosch, B. Frenz, P. J. M. Rottier, F. DiMaio, F. A. Rey, D. Veesler, Cryo-electron microscopy structure of a coronavirus spike glycoprotein trimer. *Nature* **531**, 114–117 (2016). [doi:10.1038/nature16988](https://doi.org/10.1038/nature16988) Medline
 22. Y. Yuan, D. Cao, Y. Zhang, J. Ma, J. Qi, Q. Wang, G. Lu, Y. Wu, J. Yan, Y. Shi, X. Zhang, G. F. Gao, Cryo-EM structures of MERS-CoV and SARS-CoV spike glycoproteins reveal the dynamic receptor binding domains. *Nat. Commun.* **8**, 15092 (2017). [doi:10.1038/ncomms15092](https://doi.org/10.1038/ncomms15092) Medline
 23. C. L. Hsieh, J. A. Goldsmith, J. M. Schaub, A. M. DiVenere, H.-C. Kuo, K. Javanmardi, K. C. Le, D. Wrapp, A. G. Lee, Y. Liu, C.-W. Chou, P. O. Byrne, C. K. Hjorth, N. V. Johnson, J. Ludes-Meyers, A. W. Nguyen, J. Park, N. Wang, D. Amengor, J. J. Lavinder, G. C. Ippolito, J. A. Maynard, I. J. Finkelstein, J. S. McLellan, Structure-based design of prefusion-stabilized SARS-CoV-2 spikes. *Science* **369**, 1501–1505 (2020). [doi:10.1126/science.abd0826](https://doi.org/10.1126/science.abd0826) Medline
 24. J. F. Chan, A. J. Zhang, S. Yuan, V. K. Poon, C. C. Chan, A. C. Lee, W. M. Chan, Z. Fan, H. W. Tsui, L. Wen, R. Liang, J. Cao, Y. Chen, K. Tang, C. Luo, J. P. Cai, K. H. Kok, H. Chu, K. H. Chan, S. Sridhar, Z. Chen, H. Chen, K. K. To, K. Y. Yuen, Simulation of the clinical and pathological manifestations of coronavirus disease 2019 (COVID-19) in a golden Syrian hamster model: Implications for disease pathogenesis and transmissibility. *Clin. Infect. Dis.* **71**, 2428–2446 (2020). [doi:10.1093/cid/ciaa325](https://doi.org/10.1093/cid/ciaa325) Medline
 25. M. Imai, K. Iwatsuki-Horimoto, M. Hatta, S. Loeber, P. J. Halfmann, N. Nakajima, T. Watanabe, M. Ujie, K. Takahashi, M. Ito, S. Yamada, S. Fan, S. Chiba, M. Kuroda, L. Guan, K. Takada, T. Armbrust, A. Balogh, Y. Furusawa, M. Okuda, H. Ueki, A. Yasuhara, Y. Sakai-Tagawa, T. J. S. Lopes, M. Kiso, S. Yamayoshi, N. Kinoshita, N. Ohmagari, S. I. Hattori, M. Takeda, H. Mitsuya, F. Krammer, T. Suzuki, Y. Kawaoka, Syrian hamsters as a small animal model for SARS-CoV-2 infection and countermeasure development. *Proc. Natl. Acad. Sci. U.S.A.* **117**, 16587–16595 (2020). [doi:10.1073/pnas.2009799117](https://doi.org/10.1073/pnas.2009799117) Medline
 26. S. F. Sia, L.-M. Yan, A. W. H. Chin, K. Fung, K.-T. Choy, A. Y. L. Wong, P. Kaewpreedee, R. A. P. M. Perera, L. L. M. Poon, J. M. Nicholls, M. Peiris, H.-L. Yen, Pathogenesis and transmission of SARS-CoV-2 in golden hamsters. *Nature* **583**, 834–838 (2020). [doi:10.1038/s41586-020-2342-5](https://doi.org/10.1038/s41586-020-2342-5) Medline
 27. R. Kong, K. Xu, T. Zhou, P. Acharya, T. Lemmin, K. Liu, G. Ozorowski, C. Soto, J. D. Taft, R. T. Bailer, E. M. Cale, L. Chen, C. W. Choi, G.-Y. Chuang, N. A. Doria-Rose, A. Druz, I. S. Georgiev, J. Gorman, J. Huang, M. G. Joyce, M. K. Louder, X. Ma, K. McKee, S. O'Dell, M. Pancera, Y. Yang, S. C. Blanchard, W. Mothes, D. R. Burton, W. C. Koff, M. Connors, A. B. Ward, P. D. Kwong, J. R. Mascola, Fusion peptide of HIV-1 as a site of vulnerability to neutralizing antibody. *Science* **352**, 828–833 (2016). [doi:10.1126/science.aae0474](https://doi.org/10.1126/science.aae0474) Medline
 28. K. Xu, P. Acharya, R. Kong, C. Cheng, G.-Y. Chuang, K. Liu, M. K. Louder, S. O'Dell, R. Rawi, M. Sastry, C.-H. Shen, B. Zhang, T. Zhou, M. Asokan, R. T. Bailer, M. Chambers, X. Chen, C. W. Choi, V. P. Dandey, N. A. Doria-Rose, A. Druz, E. T. Eng, S. K. Farney, K. E. Foulds, H. Geng, I. S. Georgiev, J. Gorman, K. R. Hill, A. J. Jafari, Y. D. Kwon, Y.-T. Lai, T. Lemmin, K. McKee, T. Y. Ohr, L. Ou, D. Peng, A. P. Rowshan, Z. Sheng, J.-P. Todd, Y. Tsybovsky, E. G. Viox, Y. Wang, H. Wei, Y. Yang, A. F. Zhou, R. Chen, L. Yang, D. G. Scorpio, A. B. McDermott, L. Shapiro, B. Carragher, C. S. Potter, J. R. Mascola, P. D. Kwong, Epitope-based vaccine design yields fusion peptide-directed antibodies that neutralize diverse strains of HIV-1. *Nat. Med.* **24**, 857–867 (2018). [doi:10.1038/s41591-018-0042-6](https://doi.org/10.1038/s41591-018-0042-6) Medline
 29. R. Kong, H. Duan, Z. Sheng, K. Xu, P. Acharya, X. Chen, C. Cheng, A. S. Dingens, J. Gorman, M. Sastry, C.-H. Shen, B. Zhang, T. Zhou, G.-Y. Chuang, C. W. Chao, Y. Gu, A. J. Jafari, M. K. Louder, S. O'Dell, A. P. Rowshan, E. G. Viox, Y. Wang, C. W. Choi, M. M. Corcoran, A. R. Corrigan, V. P. Dandey, E. T. Eng, H. Geng, K. E. Foulds, Y. Guo, Y. D. Kwon, B. Lin, K. Liu, R. D. Mason, M. C. Nason, T. Y. Ohr, L. Ou, R. Rawi, E. K. Sarfo, A. Schön, J. P. Todd, S. Wang, H. Wei, W. Wu, J. C. Mullikin, R. T. Bailer, N. A. Doria-Rose, G. B. Karlsson Hedestam, D. G. Scorpio, J. Overbaugh, J. D. Bloom, B. Carragher, C. S. Potter, L. Shapiro, P. D. Kwong, J. R. Mascola; NISC Comparative Sequencing Program, Antibody lineages with vaccine-induced antigen-binding hotspots develop broad HIV neutralization. *Cell* **178**, 567–584.e19 (2019). [doi:10.1016/j.cell.2019.06.030](https://doi.org/10.1016/j.cell.2019.06.030) Medline
 30. M. A. Tortorici, N. Czudnochowski, T. N. Starr, R. Marzi, A. C. Walls, F. Zatta, J. E. Bowen, S. Jaconi, J. Di Julio, Z. Wang, A. De Marco, S. K. Zepeda, D. Pinto, Z. Liu, M. Beltramello, I. Bartha, M. P. Housley, F. A. Lempp, L. E. Rosen, E. Dellot Jr., H. Kaiser, M. Montiel-Ruiz, J. Zhou, A. Addetia, B. Guarino, K. Culap, N. Sprugasci, C. Saliba, E. Vetti, I. Giacchetto-Sasselli, C. S. Fregnii, R. Abdelnabi, S. C. Foo, C. Havenar-Daughton, M. A. Schmid, F. Benigni, E. Cameroni, J. Neyts, A. Telenti, H. W. Virgin, S. P. J. Whelan, G. Snell, J. D. Bloom, D. Corti, D. Veesler, M. S. Pizzuto, Broad sarbecovirus neutralization by a human monoclonal antibody. *Nature* **597**, 103–108 (2021). [doi:10.1038/s41586-021-03817-4](https://doi.org/10.1038/s41586-021-03817-4) Medline
 31. I. Ullah, J. Prévost, M. S. Ladinsky, H. Stone, M. Lu, S. P. Anand, G. Beaudoin-Bussières, K. Symrnes, M. Benlarbi, S. Ding, R. Gasser, C. Firk, Y. Chen, A. Tauzin, G. Goyette, C. Bourassa, H. Medjahed, M. Mack, K. Chung, C. B. Wilen, G. A. Dekaban, J. D. Dikeakos, E. A. Bruce, D. E. Kaufmann, L. Stamatatos, A. T. McGuire, J. Richard, M. Pazgier, P. J. Bjorkman, W. Mothes, A. Finzi, P. Kumar, P. D. Uchil, Live imaging of SARS-CoV-2 infection in mice reveals that neutralizing antibodies require Fc function for optimal efficacy. *Immunity* **54**, 2143–2158.e15 (2021). [doi:10.1016/j.jimmuni.2021.08.015](https://doi.org/10.1016/j.jimmuni.2021.08.015) Medline
 32. R. Yamin, A. T. Jones, H.-H. Hoffmann, A. Schäfer, K. S. Kao, R. L. Francis, T. P. Sheahan, R. S. Baric, C. M. Rice, J. V. Ravetch, S. Bournazos, Fc-engineered antibody therapeutics with improved anti-SARS-CoV-2 efficacy. *Nature* **599**, 465–470 (2021). [doi:10.1038/s41586-021-04017-w](https://doi.org/10.1038/s41586-021-04017-w) Medline
 33. Y. C. Bartsch, C. Wang, T. Zohar, S. Fischinger, C. Atyeo, J. S. Burke, J. Kang, A. G. Edlow, A. Fasano, L. R. Baden, E. J. Nilles, A. E. Woolley, E. W. Karlson, A. R. Hopke, D. Irmlia, E. S. Fischer, E. T. Ryan, R. C. Charles, B. D. Julg, D. A. Lauffenburger, L. M. Yonker, G. Alter, Humoral signatures of protective and pathological SARS-CoV-2 infection in children. *Nat. Med.* **27**, 454–462 (2021). [doi:10.1038/s41591-021-01263-3](https://doi.org/10.1038/s41591-021-01263-3) Medline
 34. C. H. Shen, B. J. DeKosky, Y. Guo, K. Xu, Y. Gu, D. Kilam, S. H. Ko, R. Kong, K. Liu, M. K. Louder, L. Ou, B. Zhang, C. W. Chao, M. M. Corcoran, E. Feng, J. Huang, E. Normandin, S. O'Dell, A. Ransier, R. Rawi, M. Sastry, S. D. Schmidt, S. Wang, Y. Wang, G.-Y. Chuang, N. A. Doria-Rose, B. Lin, T. Zhou, E. A. Boritz, M. Connors, D. C. Douek, G. B. Karlsson Hedestam, Z. Sheng, L. Shapiro, J. R. Mascola, P. D. Kwong, VRC34-antibody lineage development reveals how a required rare mutation shapes the maturation of a broad HIV-neutralizing lineage. *Cell Host Microbe* **27**, 531–543.e6 (2020). [doi:10.1016/j.chom.2020.01.027](https://doi.org/10.1016/j.chom.2020.01.027) Medline
 35. S. Kratochvil, C.-H. Shen, Y.-C. Lin, K. Xu, U. Nair, L. Da Silva Pereira, P. Tripathi, J. Arnold, G.-Y. Chuang, E. Melzi, A. Schön, B. Zhang, M. Dillon, B. Bonilla, B. J. Flynn, K. H. Kirsch, N. K. Kisalu, P. K. Kiyuka, T. Liu, L. Ou, M. Pancera, R. Rawi, M. Reveiz, K. Seignon, L. T. Wang, M. T. Waring, J. Warner, Y. Yang, J. R. Francica, A. H. Idris, R. A. Seder, P. D. Kwong, F. D. Batista, Vaccination in a humanized mouse model elicits highly protective PfcSP-targeting anti-malarial antibodies. *Immunity* **54**, 2859–2876.e7 (2021). [doi:10.1016/j.jimmuni.2021.10.017](https://doi.org/10.1016/j.jimmuni.2021.10.017) Medline
 36. A. Wellner, C. McMahon, M. S. A. Gilman, J. R. Clements, S. Clark, K. M. Nguyen, M. H. Ho, V. J. Hu, J.-E. Shin, J. Feldman, B. M. Hauser, T. M. Caradonna, L. M. Wingler, A. G. Schmidt, D. S. Marks, J. Abraham, A. C. Kruse, C. C. Liu, Rapid generation of potent antibodies by autonomous hypermutation in yeast. *Nat. Chem. Biol.* **17**, 1057–1064 (2021). [doi:10.1038/s41589-021-00832-4](https://doi.org/10.1038/s41589-021-00832-4) Medline
 37. C. M. Poh, G. Carissimo, B. Wang, S. N. Amrun, C. Y.-P. Lee, R. S.-L. Chee, S.-W. Fong, N. K.-W. Yeo, W.-H. Lee, A. Torres-Ruesta, Y.-S. Leo, M. I.-C. Chen, S.-Y. Tan, L. Y. A. Chai, S. Kalimuddin, S. S. G. Kheng, S.-Y. Thien, B. E. Young, D. C. Lye, B. J. Hanson, C.-I. Wang, L. Renia, L. F. P. Ng, Two linear epitopes on the SARS-CoV-2

- spike protein that elicit neutralising antibodies in COVID-19 patients. *Nat. Commun.* **11**, 2806 (2020). doi:[10.1038/s41467-020-16638-2](https://doi.org/10.1038/s41467-020-16638-2) Medline
38. W. R. Morgenlander, S. N. Henson, D. R. Monaco, A. Chen, K. Littlefield, E. M. Bloch, E. Fujimura, I. Ruczinski, A. R. Crowley, H. Natarajan, S. E. Butler, J. A. Weiner, M. Z. Li, T. S. Bonny, S. E. Benner, A. Balagopal, D. Sullivan, S. Shoham, T. C. Quinn, S. H. Eshleman, A. Casadevall, A. D. Redd, O. Laeyendecker, M. E. Ackerman, A. Pekosz, S. J. Elledge, M. Robinson, A. A. R. Tobian, H. B. Larman, Antibody responses to endemic coronaviruses modulate COVID-19 convalescent plasma functionality. *J. Clin. Invest.* **131**, e146927 (2021). doi:[10.1172/JCI146927](https://doi.org/10.1172/JCI146927) Medline
39. X. Sun *et al.*, Novel neutralization mechanism of a human antibody with pan-coronavirus reactivity. *Res Sq.* [Preprint] (2021); <https://doi.org/10.21203/rs.3.rs-952553/v1>
40. N. Vanderheijden, A. Stevaert, J. Xie, X. Ren, C. Barbezange, S. Noppen, I. Desombere, B. Verhasselt, P. Geldhof, N. Vereecke, V. Stroobants, D. Oh, M. Vanhee, L. M. J. Naesens, H. J. Nauwynck, Functional analysis of human and feline coronavirus cross-reactive antibodies directed against the SARS-CoV-2 fusion peptide. *Front. Immunol.* **12**, 790415 (2022). doi:[10.3389/fimmu.2021.790415](https://doi.org/10.3389/fimmu.2021.790415) Medline
41. C. Dreyfus, N. S. Laursen, T. Kwaks, D. Zuidgeest, R. Khayat, D. C. Ekiert, J. H. Lee, Z. Metlagel, M. V. Bujny, M. Jongeneelen, R. van der Vlugt, M. Lamrani, H. J. W. M. Korse, E. Geelen, Ö. Sahin, M. Sieuwerts, J. P. J. Brakenhoff, R. Vogels, O. T. W. Li, L. L. M. Poon, M. Peiris, W. Koudstaal, A. B. Ward, I. A. Wilson, J. Goudsmit, R. H. E. Friesen, Highly conserved protective epitopes on influenza B viruses. *Science* **337**, 1343–1348 (2012). doi:[10.1126/science.1222908](https://doi.org/10.1126/science.1222908) Medline
42. T. F. Rogers, F. Zhao, D. Huang, N. Beutler, A. Burns, W. T. He, O. Limbo, C. Smith, G. Song, J. Woehl, L. Yang, R. K. Abbott, S. Callaghan, E. Garcia, J. Hurtado, M. Parren, L. Peng, S. Ramirez, J. Ricketts, M. J. Ricciardi, S. A. Rawlings, N. C. Wu, M. Yuan, D. M. Smith, D. Nemazee, J. R. Teijaro, J. E. Voss, I. A. Wilson, R. Andrabí, B. Briney, E. Landais, D. Sok, J. G. Jardine, D. R. Burton, Isolation of potent SARS-CoV-2 neutralizing antibodies and protection from disease in a small animal model. *Science* **369**, 956–963 (2020). doi:[10.1126/science.abc7520](https://doi.org/10.1126/science.abc7520) Medline
43. L. T. Wang, L. S. Pereira, Y. Flores-Garcia, J. O'Connor, B. J. Flynn, A. Schön, N. K. Hurlburt, M. Dillon, A. S. P. Yang, A. Fabra-Garcia, A. H. Idris, B. T. Mayer, M. W. Gerber, R. Gottardo, R. D. Mason, N. Cavett, R. B. Ballard, N. K. Kisalu, A. Molina-Cruz, J. Nelson, R. Vistein, C. Barillas-Mury, R. Amino, D. Baker, N. P. King, R. W. Sauerwein, M. Pancera, I. A. Cockburn, F. Zavala, J. R. Francia, R. A. Seder, A potent anti-malarial human monoclonal antibody targets circumsporozoite protein minor repeats and neutralizes sporozoites in the liver. *Immunity* **53**, 733–744.e8 (2020). doi:[10.1016/j.jimmuni.2020.08.014](https://doi.org/10.1016/j.jimmuni.2020.08.014) Medline
44. E. Krissinel, K. Henrick, Inference of macromolecular assemblies from crystalline state. *J. Mol. Biol.* **372**, 774–797 (2007). doi:[10.1016/j.jmb.2007.05.022](https://doi.org/10.1016/j.jmb.2007.05.022) Medline
45. S. Bangaru, A. Antanasijevic, N. Kose, L. M. Sewall, A. M. Jackson, N. Suryadevara, X. Zhan, J. L. Torres, J. Copps, A. T. de la Peña, J. E. Crowe Jr., A. B. Ward, Structural mapping of antibody landscapes to human betacoronavirus spike proteins. *Sci. Adv.* **8**, eabn2911 (2022). doi:[10.1126/sciadv.abn2911](https://doi.org/10.1126/sciadv.abn2911) Medline
46. H. Lv, O. T.-Y. Tsang, R. T. Y. So, Y. Wang, M. Yuan, H. Liu, G. K. Yip, Q. W. Teo, Y. Lin, W. Liang, J. Wang, W. W. Ng, I. A. Wilson, J. S. M. Peiris, N. C. Wu, C. K. P. Mok, Homologous and heterologous serological response to the N-terminal domain of SARS-CoV-2 in humans and mice. *Eur. J. Immunol.* **51**, 2296–2305 (2021). doi:[10.1002/eji.202149234](https://doi.org/10.1002/eji.202149234) Medline
47. M. Yuan, N. C. Wu, X. Zhu, C. D. Lee, R. T. Y. So, H. Lv, C. K. P. Mok, I. A. Wilson, A highly conserved cryptic epitope in the receptor binding domains of SARS-CoV-2 and SARS-CoV. *Science* **368**, 630–633 (2020). doi:[10.1126/science.abb7269](https://doi.org/10.1126/science.abb7269) Medline
48. D. C. Ekiert, G. Bhabha, M.-A. Elsiger, R. H. E. Friesen, M. Jongeneelen, M. Throsby, J. Goudsmit, I. A. Wilson, Antibody recognition of a highly conserved influenza virus epitope. *Science* **324**, 246–251 (2009). doi:[10.1126/science.1171491](https://doi.org/10.1126/science.1171491) Medline
49. C. Crosnier, M. Wanaguru, B. McDade, F. H. Osier, K. Marsh, J. C. Rayner, G. J. Wright, A library of functional recombinant cell-surface and secreted *P. falciparum* merozoite proteins. *Mol. Cell. Proteomics* **12**, 3976–3986 (2013). doi:[10.1074/mcp.O113.028357](https://doi.org/10.1074/mcp.O113.028357) Medline
50. J. Huang, N. A. Doria-Rose, N. S. Longo, L. Laub, C.-L. Lin, E. Turk, B. H. Kang, S. A. Migueles, R. T. Bailer, J. R. Mascola, M. Connors, Isolation of human monoclonal antibodies from peripheral blood B cells. *Nat. Protoc.* **8**, 1907–1915 (2013). doi:[10.1038/nprot.2013.117](https://doi.org/10.1038/nprot.2013.117) Medline
51. S. Moir, R. Lapointe, A. Malaspina, M. Ostrowski, C. E. Cole, T.-W. Chun, J. Adelsberger, M. Baseler, P. Hwu, A. S. Fauci, CD40-Mediated induction of CD4 and CXCR4 on B lymphocytes correlates with restricted susceptibility to human immunodeficiency virus type 1 infection: Potential role of B lymphocytes as a viral reservoir. *J. Virol.* **73**, 7972–7980 (1999). doi:[10.1128/JVI.73.10.7972-7980.1999](https://doi.org/10.1128/JVI.73.10.7972-7980.1999) Medline
52. T. Tiller, E. Meffre, S. Yurasov, M. Tsuji, M. C. Nussenzweig, H. Wardemann, Efficient generation of monoclonal antibodies from single human B cells by single cell RT-PCR and expression vector cloning. *J. Immunol. Methods* **329**, 112–124 (2008). doi:[10.1016/j.jim.2007.09.017](https://doi.org/10.1016/j.jim.2007.09.017) Medline
53. M. P. Lefranc, Immunoglobulin and T cell receptor genes: IMGT® and the birth and rise of immunoinformatics. *Front. Immunol.* **5**, 22 (2014). doi:[10.3389/fimmu.2014.00022](https://doi.org/10.3389/fimmu.2014.00022) Medline
54. K. Katoh, J. Rozewicki, K. D. Yamada, MAFFT online service: Multiple sequence alignment, interactive sequence choice and visualization. *Brief. Bioinform.* **20**, 1160–1166 (2019). doi:[10.1093/bib/bbx108](https://doi.org/10.1093/bib/bbx108) Medline
55. I. Letunic, P. Bork, Interactive Tree Of Life (iTOL) v5: An online tool for phylogenetic tree display and annotation. *Nucleic Acids Res.* **49**, W293–W296 (2021). doi:[10.1093/nar/gkab301](https://doi.org/10.1093/nar/gkab301) Medline
56. G. E. Crooks, G. Hon, J. M. Chandonia, S. E. Brenner, WebLogo: A sequence logo generator. *Genome Res.* **14**, 1188–1190 (2004). doi:[10.1101/gr.849004](https://doi.org/10.1101/gr.849004) Medline
57. J. Schindelin, I. Arganda-Carreras, E. Frise, V. Kaynig, M. Longair, T. Pietzsch, S. Preibisch, C. Rueden, S. Saalfeld, B. Schmid, J.-Y. Tinevez, D. J. White, V. Hartenstein, K. Eliceiri, P. Tomancak, A. Cardona, Fiji: An open-source platform for biological-image analysis. *Nat. Methods* **9**, 676–682 (2012). doi:[10.1038/nmeth.2019](https://doi.org/10.1038/nmeth.2019) Medline
58. L. Lu, Q. Liu, Y. Zhu, K.-H. Chan, L. Qin, Y. Li, Q. Wang, J. F.-W. Chan, L. Du, F. Yu, C. Ma, S. Ye, K.-Y. Yuen, R. Zhang, S. Jiang, Structure-based discovery of Middle East respiratory syndrome coronavirus fusion inhibitor. *Nat. Commun.* **5**, 3067 (2014). doi:[10.1038/ncomms4067](https://doi.org/10.1038/ncomms4067) Medline
59. E. Davidson, B. J. Doranz, A high-throughput shotgun mutagenesis approach to mapping B-cell antibody epitopes. *Immunology* **143**, 13–20 (2014). doi:[10.1111/imm.12323](https://doi.org/10.1111/imm.12323) Medline
60. Z. Otwinowski, W. Minor, Processing of X-ray diffraction data collected in oscillation mode. *Methods Enzymol.* **276**, 307–326 (1997). doi:[10.1016/S0076-6879\(97\)76066-X](https://doi.org/10.1016/S0076-6879(97)76066-X) Medline
61. A. J. McCoy, R. W. Grosse-Kunstleve, P. D. Adams, M. D. Winn, L. C. Storoni, R. J. Read, Phaser crystallographic software. *J. Appl. Crystallogr.* **40**, 658–674 (2007). doi:[10.1107/S0021889807021206](https://doi.org/10.1107/S0021889807021206) Medline
62. P. Emsley, B. Lohkamp, W. G. Scott, K. Cowtan, Features and development of Coot. *Acta Crystallogr. D* **66**, 486–501 (2010). doi:[10.1107/S0907444910007493](https://doi.org/10.1107/S0907444910007493) Medline
63. P. D. Adams, P. V. Afonine, G. Bunkóczki, V. B. Chen, I. W. Davis, N. Echols, J. J. Headd, L.-W. Hung, G. J. Kapral, R. W. Grosse-Kunstleve, A. J. McCoy, N. W. Moriarty, R. Oeffner, R. J. Read, D. C. Richardson, J. S. Richardson, T. C. Terwilliger, P. H. Zwart, PHENIX: A comprehensive Python-based system for macromolecular structure solution. *Acta Crystallogr. D* **66**, 213–221 (2010). doi:[10.1107/S0907444909052925](https://doi.org/10.1107/S0907444909052925) Medline
64. D. H. Barouch, Z. Y. Yang, W. P. Kong, B. Korioth-Schmitz, S. M. Sumida, D. M. Truitt, M. G. Kishko, J. C. Arthur, A. Miura, J. R. Mascola, N. L. Letvin, G. J. Nabel, A human T-cell leukemia virus type 1 regulatory element enhances the immunogenicity of human immunodeficiency virus type 1 DNA vaccines in mice and nonhuman primates. *J. Virol.* **79**, 8828–8834 (2005). doi:[10.1128/JVI.79.14.8828-8834.2005](https://doi.org/10.1128/JVI.79.14.8828-8834.2005) Medline
65. L. Naldini, U. Blömer, F. H. Gage, D. Trono, I. M. Verma, Efficient transfer, integration, and sustained long-term expression of the transgene in adult rat brains injected with a lentiviral vector. *Proc. Natl. Acad. Sci. U.S.A.* **93**, 11382–11388 (1996). doi:[10.1073/pnas.93.21.11382](https://doi.org/10.1073/pnas.93.21.11382) Medline
66. L. Wang, W. Shi, M. G. Joyce, K. Modjarrad, Y. Zhang, K. Leung, C. R. Lees, T. Zhou, H. M. Yassine, M. Kanekiyo, Z. Y. Yang, X. Chen, M. M. Becker, M. Freeman, L. Vogel, J. C. Johnson, G. Olinger, J. P. Todd, U. Bagci, J. Solomon, D. J. Mollura, L. Hensley, P. Jahrling, M. R. Denison, S. S. Rao, K. Subbarao, P. D. Kwong, J. R. Mascola, W.-P. Kong, B. S. Graham, Evaluation of candidate vaccine approaches

- for MERS-CoV. *Nat. Commun.* **6**, 7712 (2015). doi:[10.1038/ncomms8712](https://doi.org/10.1038/ncomms8712) Medline
67. E. M. Covés-Datson, J. Dyall, L. E. DeWald, S. R. King, D. Dube, M. Legendre, E. Nelson, K. C. Drews, R. Gross, D. M. Gerhardt, L. Torzewski, E. Postnikova, J. Y. Liang, B. Ban, J. Shetty, L. E. Hensley, P. B. Jahrling, G. G. Olinger Jr., J. M. White, D. M. Markovitz, Inhibition of Ebola virus by a molecularly engineered banana lectin. *PLOS Negl. Trop. Dis.* **13**, e0007595 (2019). doi:[10.1371/journal.pntd.0007595](https://doi.org/10.1371/journal.pntd.0007595) Medline
68. M. Matrosovich, T. Matrosovich, W. Garten, H. D. Klenk, New low-viscosity overlay medium for viral plaque assays. *Virol. J.* **3**, 63 (2006). doi:[10.1186/1743-422X-3-63](https://doi.org/10.1186/1743-422X-3-63) Medline
69. Y. Cai, J. Zhang, T. Xiao, H. Peng, S. M. Sterling, R. M. Walsh Jr., S. Rawson, S. Rits-Volloch, B. Chen, Distinct conformational states of SARS-CoV-2 spike protein. *Science* **369**, 1586–1592 (2020). doi:[10.1126/science.abb4251](https://doi.org/10.1126/science.abb4251) Medline

ACKNOWLEDGMENTS

We thank the blood sample donors at the New York Blood Center; Sandhya Bangaru, Gabriel Ozorowski, Alba Torrents de la Peña, and Andrew Ward for providing HCoV-OC43 and MERS-CoV; Gavin Wright and Nicole Muller-Sieneth (Wright lab, University of York) for providing recombinant CD4; Lawrence Wang and Robert Seder for providing the L9 antibody; Melanie Cohen and Julie Laux for assistance with cell sorting. We thank Nick Vaughan, Kurt Cooper, Becky Reeder, Marisa St Claire, Kyra Hadley, David Drawbaugh, Amanda Hischak, Randy Hart, Nejra Isic, Michael Murphy, Elena Postnikova, Manu Anantpadma and Elizabeth Eudy for assistance with hamster experiments. We are grateful to the staff of Advanced Photon Source and Stanford Synchrotron Radiation Lightsource (SSRL) Beamline 12-1 for assistance with synchrotron data collection. **Funding:** Supported by the Division of Intramural Research and the Vaccine Research Center, National Institute of Allergy and Infectious Diseases (NIAID), National Institutes of Health (NIH). (ID, SM, JWY, PDC, MRH, JRM, JT). This project has been funded in whole or in part with Federal funds from the National Institute of Allergy and Infectious Diseases (NIAID), National Institutes of Health (NIH), U.S. Department of Health and Human Services (DHHS) under Contract No. HHSN272201800013C. NIH grant R01AI132317 (DN and LP), HHSN contract 75N93019C00073 (JKW and ED), and the Bill and Melinda Gates Foundation grant INV-004923 (IAW). This research used resources of the Advanced Photon Source; a U.S. Department of Energy (DOE) Office of Science User Facility operated for the DOE Office of Science by Argonne National Laboratory under Contract No. DE-AC02-06CH11357. GM/CA@APS has been funded by the National Cancer Institute (ACB-12002) and the National Institute of General Medical Sciences (AGM-12006, P30GM138396). Extraordinary facility operations were supported in part by the DOE Office of Science through the National Virtual Biotechnology Laboratory, a consortium of DOE national laboratories focused on the response to COVID-19, with funding provided by the Coronavirus CARES Act. Use of the Stanford Synchrotron Radiation Lightsource, SLAC National Accelerator Laboratory, is supported by the U.S. Department of Energy, Office of Science, Office of Basic Energy Sciences under Contract No. DE-AC02-76SF00515. The SSRL Structural Molecular Biology Program is supported by the DOE Office of Biological and Environmental Research, and by the National Institutes of Health, National Institute of General Medical Sciences (P30GM133894). **Author contributions:** Conceptualization: JT, CD. Methodology: CD, CT, LPe, C-CDL, THL, MY, YC, LW, DD, BE, IK, ZH, RW, AP, ED, DG, ID, SM. Formal analysis: CD, CT, LPe, MY, YC, LW, C-CDL, THL, C-WP, JS, ED. Data curation: MP. Investigation: CD, CT, LPe, MY, LW, C-CDL, LPu, C-WP, JKW, THL, MZ, MP, DM, AC, SD, EK, LH, DP, RB, SL, DD, BE, YZ, ESY, MC, KL. Resources: RW, SM. Writing - original draft: CD, CT, MY, JT. Writing - review & editing: all authors. Visualization: CD, CT, LPe, MY, YC, LW, C-CDL, JKW, ED, JT. Supervision: ED, DG, SM, JWY, CS, PDC, DN, MRH, JRM, IAW, JT. Funding acquisition: CS, PDC, DN, MRH, JRM, IAW, JT. **Competing interests:** JT and CD are co-inventors on a provisional patent (U.S. Patent Application No. 63/308,898) filed on the mAbs described in this study. JKW and ED are employees of Integral Molecular. YC, SD, EK, LMH, DLP, RB, SL, DD, BE and MRH performed this work as employees of Laulima Government Solutions, LLC. The content of this publication does not necessarily reflect the views or policies of the DHHS or of the institutions and companies with which the authors are affiliated. All other authors declare no competing interests. **Data and materials**

availability: All data associated with this manuscript are available in the main text or the supplementary materials. Crystal structures have been deposited into the Protein Data Bank (PDB 8D36 for COV44-62, 8DAO for COV44-79 and 8D6Z for COV91-27). Antibody sequences have been deposited in GenBank under accession numbers ON695901-ON695912. Materials described in this manuscript will be available through a material transfer agreement (MTA) with the National Institute of Allergy and Infectious Diseases. **License information:** This work is licensed under a Creative Commons Attribution 4.0 International (CC BY 4.0) license, which permits unrestricted use, distribution, and reproduction in any medium, provided the original work is properly cited. To view a copy of this license, visit <https://creativecommons.org/licenses/by/4.0/>. This license does not apply to figures/photos/artwork or other content included in the article that is credited to a third party; obtain authorization from the rights holder before using such material.

SUPPLEMENTARY MATERIALS

science.org/doi/10.1126/science.abq3773

Materials and Methods

Figs. S1 to S8

Tables S1 and S2

References (45–69)

MDAR Reproducibility Checklist

Submitted 4 April 2022; accepted 6 July 2022

Published online 12 July 2022

10.1126/science.abq3773

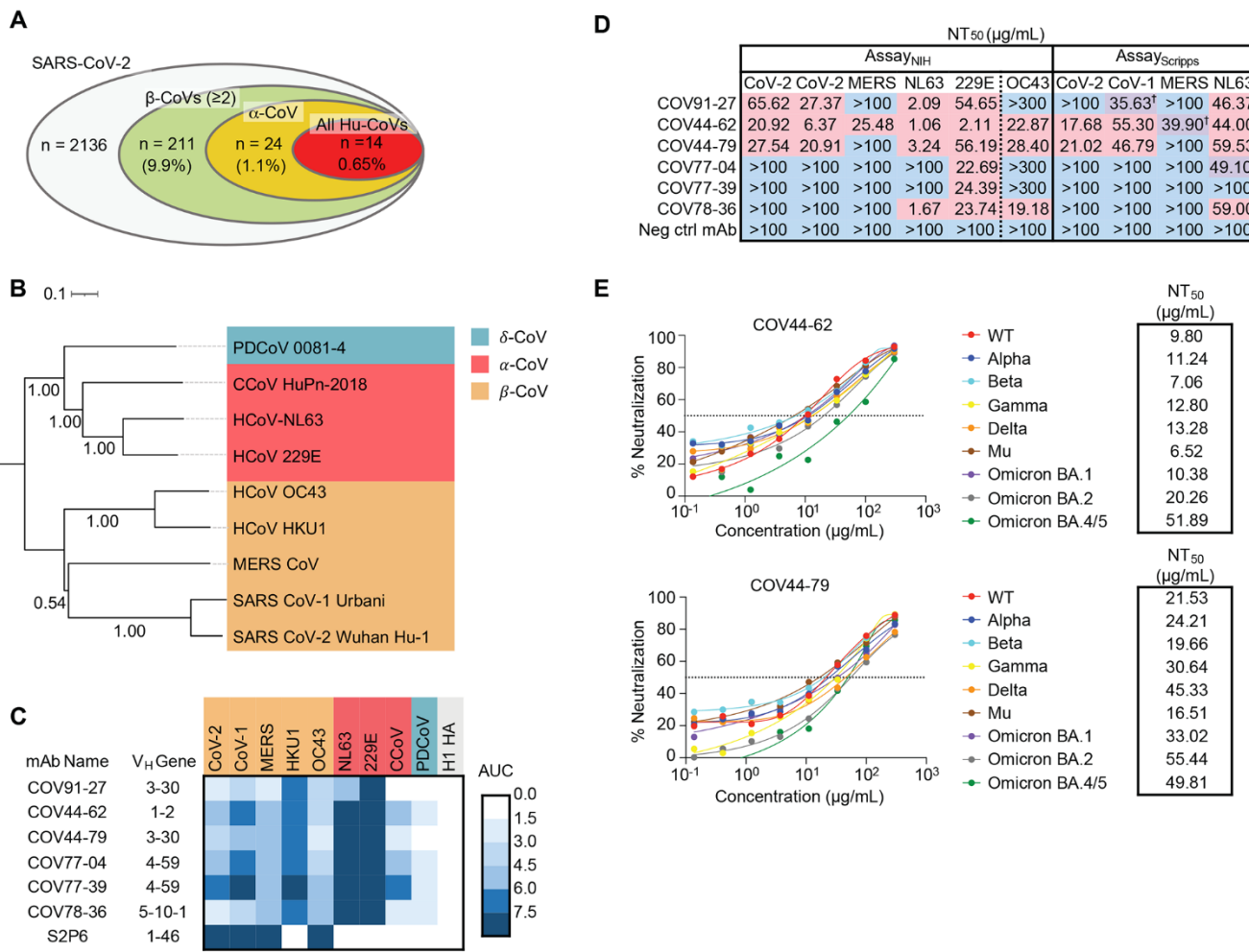


Fig. 1. Broadly neutralizing antibodies target coronaviruses associated with human disease. (A) Analysis of the frequency of MBCs expressing broadly reactive antibodies from $n = 19$ donors. Values in parentheses represent the percentage of SARS-CoV-2 reactive supernatants that also bind the specified subsets of non-SARS coronavirus spikes. A total of 10,356 MBC culture supernatants (50–100 B cells/well) was screened. (B) Phylogenetic relationships across the coronavirus spike proteins targeted by the broadly reactive mAbs were inferred by the Neighbor-Joining method in MEGA11 using full-length amino-acid sequences of CoV spike proteins. Branch lengths are drawn to scale and bootstrap values from 500 samplings are shown on the branches. The scale bar represents the number of amino acid substitutions per site. (C) Heat map representing the binding of broadly reactive mAbs to spike proteins from coronaviruses across the alpha, beta and deltacoronavirus genera. H1 hemagglutinin was included as a negative control for mAb binding experiments and area under the curve (AUC) values for each antigen are shown after subtraction with values for the negative control antigen CD4. (D) Values represent antibody titer at 50% neutralization (NT₅₀) against SARS-CoV-2 Wuhan Hu-1, SARS-CoV-1, MERS-CoV, HCoV-NL63 and HCoV-229E envelope-pseudotyped lentivirus, as well as authentic HCoV-OC43. For Assay_{NIH}, values are average of two experiments. For values with the † symbol, one NT₅₀ was determinable and one was not (i.e., >100 $\mu\text{g/mL}$), and the determinable NT₅₀ is shown. Negative controls mAbs were anti-CoV-2 RBD CV503 (for OC43 assay) (20), anti-influenza HA CR9114 (for Assay_{NIH} except OC43) (41) and anti-dengue DEN3 (for Assay_{Scripps}) (42). NT₅₀ values were calculated using the dose-response-inhibition model with 5-parameter Hill slope equation in GraphPad Prism 9. (E) Neutralization of SARS-CoV-2 variants of concern (pseudovirus) by COV44-62 and COV44-79.

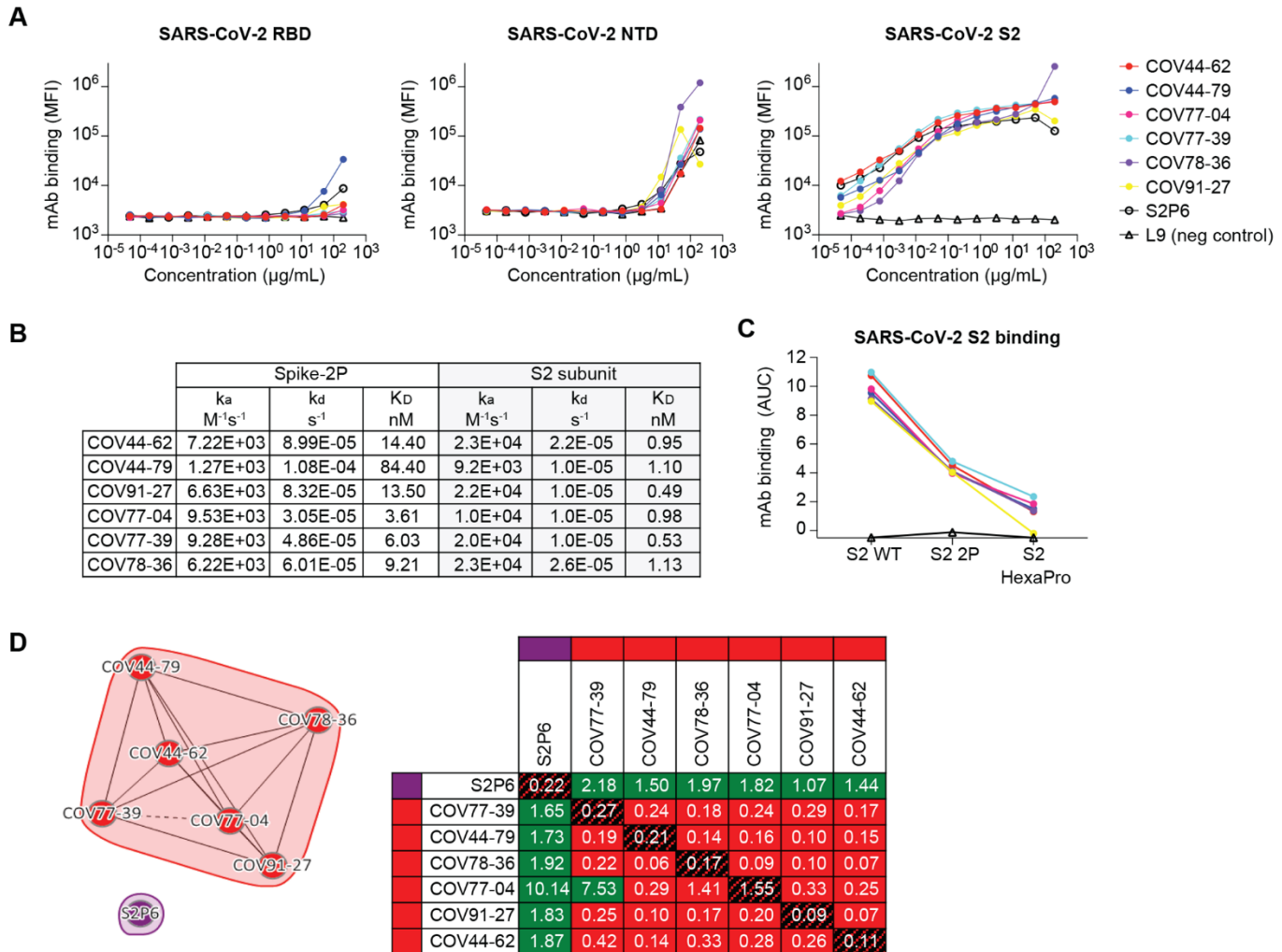
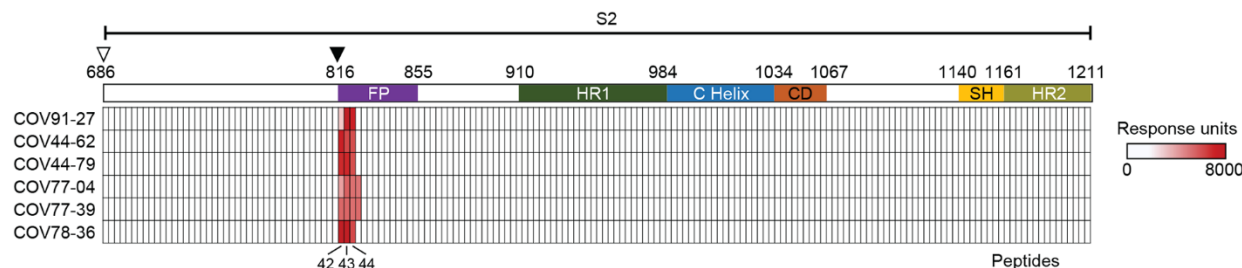


Fig. 2. Broadly reactive mAbs target the same region within the SARS-CoV-2 S2 subunit. (A) Titration curves for mAb binding to selected regions within the SARS-CoV-2 spike protein: the receptor binding domain (RBD), N-terminal domain (NTD) and the S2 subunit. Interconnected data points are shown without curve fitting. L9 is a malaria-specific mAb used as a negative control (43). (B) On-rates, off-rates and dissociation constants of the six fusion peptide Fabs for binding to SARS-CoV-2 pre-fusion stabilized spike (2P) with an unmodified furin cleavage site and the non-stabilized S2 subunit. (C) Fusion peptide mAb binding (AUC) to wild-type SARS-CoV-2 S2 subunit and S2 subunit constructs modified with two (2P) or six (HexaPro) stabilizing proline mutations. (D) Epitope binning of broadly reactive antibodies versus the S2 stem-helix targeting mAb S2P6. All included antibodies were tested as both ligands and analytes. Solid lines indicate two-way competition while hashed lines indicate one-way competition. Red boxes indicate competing antibody pairs, green boxes indicate non-competing antibody pairs and hashed filling indicates self-competition.

A**B**

	FP
CCoV-HuPn-2018	KRK Y R S A I E D L I F D K V T S G L S T V D A D Y K R C T GG
HCoV-229E	R V A G R S A I E D L I F D K V T S G L S T V D A D Y K R C T KG
HCoV-NL63	R I A G R S A I E D L I F D K V T S G L S T V D A D Y K R C T KG
HCoV-HKU1	-S S S R S A I E D L I F D K V T L S D G C F V E A -Y N N C T GG
HCoV-OC43	K A S S R S A I E D L I F D K V T L S D G C F V E A -Y N N C T GG
Mouse Hepatitis Virus	A I R G R S A I E D L I F D K V T L S D G C F V E A -Y N N C T GG
BiCoV-HKU3	K P T K R S F I E D L I F N K V T L A D C F M K Q -Y G D L GD
BiCoV-RatG13	K P T K R S F I E D L I F N K V T L A D C F M K Q -Y G E L GD
BiCoV-WIV1	K P T K R S F I E D L I F N K V T L A D C F M K Q -Y G E L GD
Civet SARS-CoV-007/2004	K P T K R S F I E D L I F N K V T L A D C F M K Q -Y G E L GD
PCoV-GX/P2V	K P T K R S F I E D L I F N K V T L A D C F M K Q -Y G D L GD
SARS-CoV-1 Urbani	K P T K R S F I E D L I F N K V T L A D C F M K Q -Y G D L GD
SARS-CoV-2 Wuhan Hu-1	K P T K R S F I E D L I F N K V T L A D C F M K Q -Y G D L GD
β	B.1.1.7 B.1.351 P.1 B.1.617.2 BA 1 BA 2 BA 2.12.1 BA 4/5
γ	BiCoV-HKU4 MERS-CoV-EMC/2012 BiCoV-HKU9
δ	AlBV AlBV-Beaudette TCoV WhaleCoV-SW1 BuCoV-HKU11-796 MuCoV-HKU13-3514 PDCoV-0081-4/2014 PDCoV-0329-4/2015 ThCoV-HKU12-600 WiCoV-HKU20

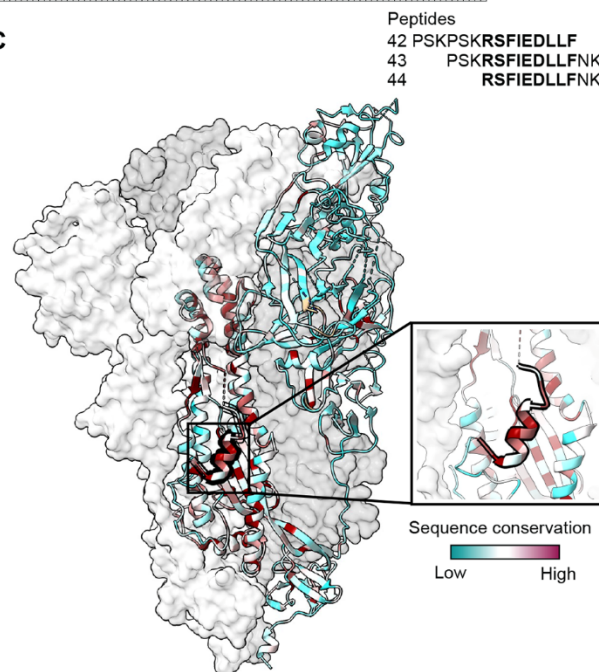
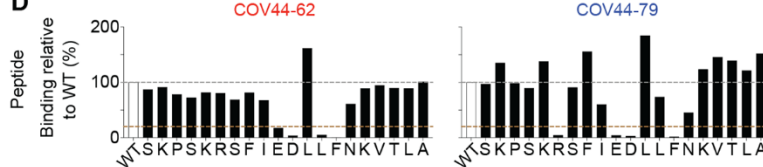
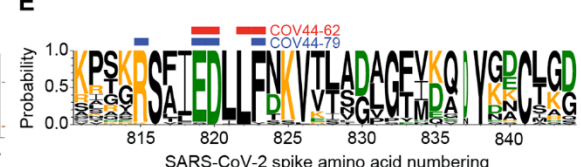
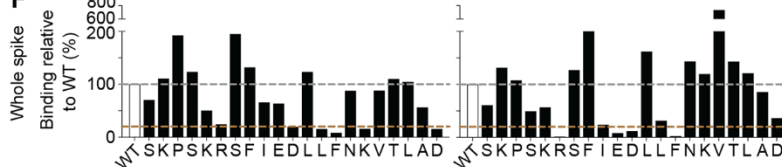
C**D****E****F**

Fig. 3 (see previous page). Broadly neutralizing antibodies target the conserved fusion peptide. (A) Heat map of SARS-CoV-2 S2 peptide array. Binding responses were assessed by SPR using a 15-mer peptide array with 12 aa overlay covering the entire S2 subunit. Each column within the map represents a single peptide. The white triangle shows the S1/S2 cleavage site and the black triangle indicates the S2' cleavage site. FP, fusion peptide; HR1, heptad repeat 1; C helix, central helix; CD, connector domain; SH, stem helix; HR2, heptad repeat 2. (B) Sequence alignment of the fusion peptide from 34 viral isolates representing a diverse group of coronaviruses across four genera. Performed using MAFFT v7.450 using a BLOSUM62 scoring matrix and the L-INS-I algorithm. (C) Sequence conservation of pre-fusion SARS-CoV-2 spike protein (PDB 6VSB) with the fusion peptide (aa 816-843) highlighted in a black outline. Inset shows a magnified view of this region. (D) Alanine scan evaluating the binding of COV44-62 and COV44-79 to the SARS-CoV2 fusion peptide. Responses were normalized to the wild-type sequence. A cut-off of 20% (brown hashed line) was used to identify residues that were critical for binding. (E) Sequence logo plot of diversity within the fusion peptide region of coronaviruses from 34 isolates, built using WebLogo 3. Height is proportional to the probability of an amino acid at a given position and amino-acid residues are colored by charge. Narrow stacks (amino acids) indicate deletions or gaps in the sequences. Numbering is based on the SARS-CoV-2 Wuhan-Hu-1 sequence. The key residues in the epitope footprints of mAbs COV44-62 (red) and COV44-79 (blue), based on peptide alanine scanning, are highlighted above the logo plot. (F) Amino acids critical for the binding of COV44-62 and COV44-79 identified by shotgun alanine mutagenesis of S2 residues on whole spike protein. Only fusion peptide residues are shown here. Key residues were identified based on a <20% signal relative to wild-type spike (brown hashed line), with no corresponding loss of signal for a control mAb, which targets the spike protein but does not bind to this site (see fig. S3C).

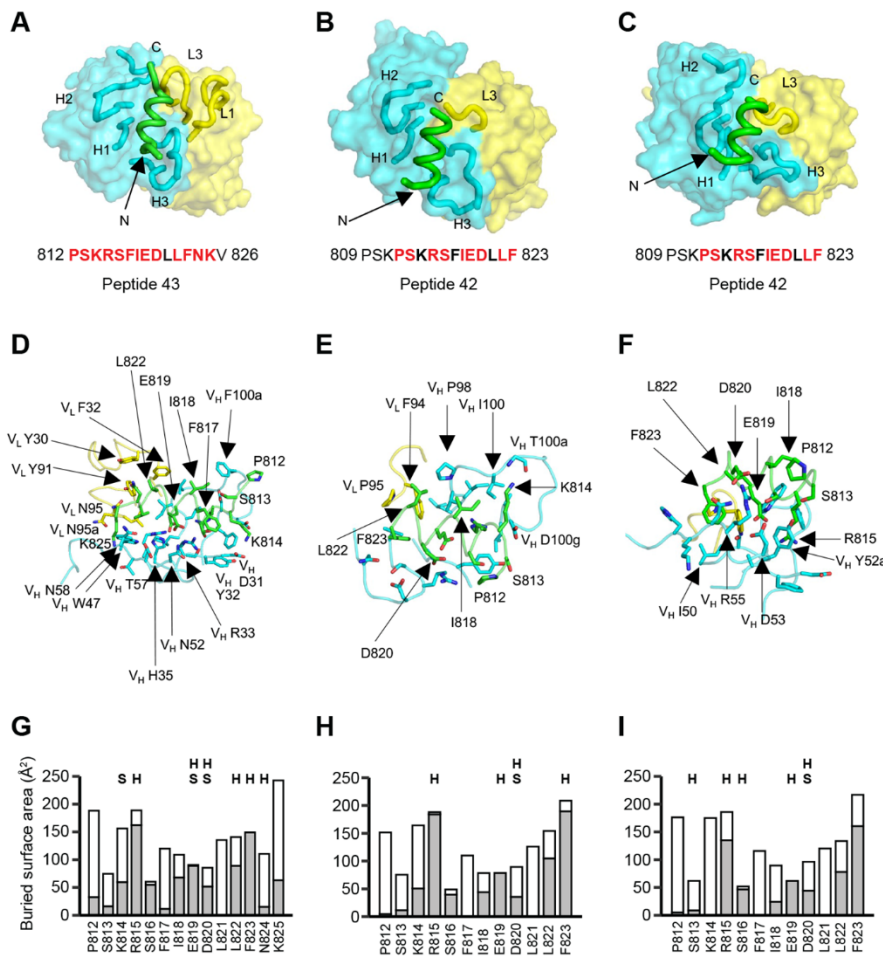


Fig. 4. Crystal structures of COV44-62, COV44-79, and COV91-27 in complex with SARS-CoV-2 fusion peptide. (A to C) The overall interactions of (A) COV44-62, (B) COV44-79, and (C) COV91-27 with the fusion peptide. Fabs are shown in a molecular surface and the CDRs and peptides are represented as tubes. Cyan and yellow represent the heavy and light chains of the Fabs. Peptides are shown in green. H1, H2, H3, L1, and L3 denotes CDRs in the heavy (H) and light (L) chains. The resolution of the crystal structures are 1.46 Å, 2.8 Å, and 2.3 Å for the COV44-62, COV44-79, and COV91-27 complexes. Peptide residues observed in the crystal structure are in bold and residues involved in interaction with antibody (buried surface area >0 Å²) are in red. (D to F) Details of the interactions between (D) COV44-62, (E) COV44-79, and (F) COV91-27 with the fusion peptide. V_H and V_L indicate the variable domains of the heavy (H) and light (L) chains. Kabat numbering was used for the Fabs and numbering in the native spike protein for the fusion peptide. The colors for the heavy chain, light chain, and fusion peptide are as in (A). (G to I) Buried surface area (in gray) and accessible surface area (in white) of each residue of the fusion peptide in complex with antibody are shown in the stacked bar chart. Residues that form polar interactions with COV44-62, COV44-79, and COV91-27 are denoted with “H” if they form a hydrogen-bond or “S” for a salt bridge on top of the corresponding bar. Buried and accessible surface areas were calculated with PISA (44).

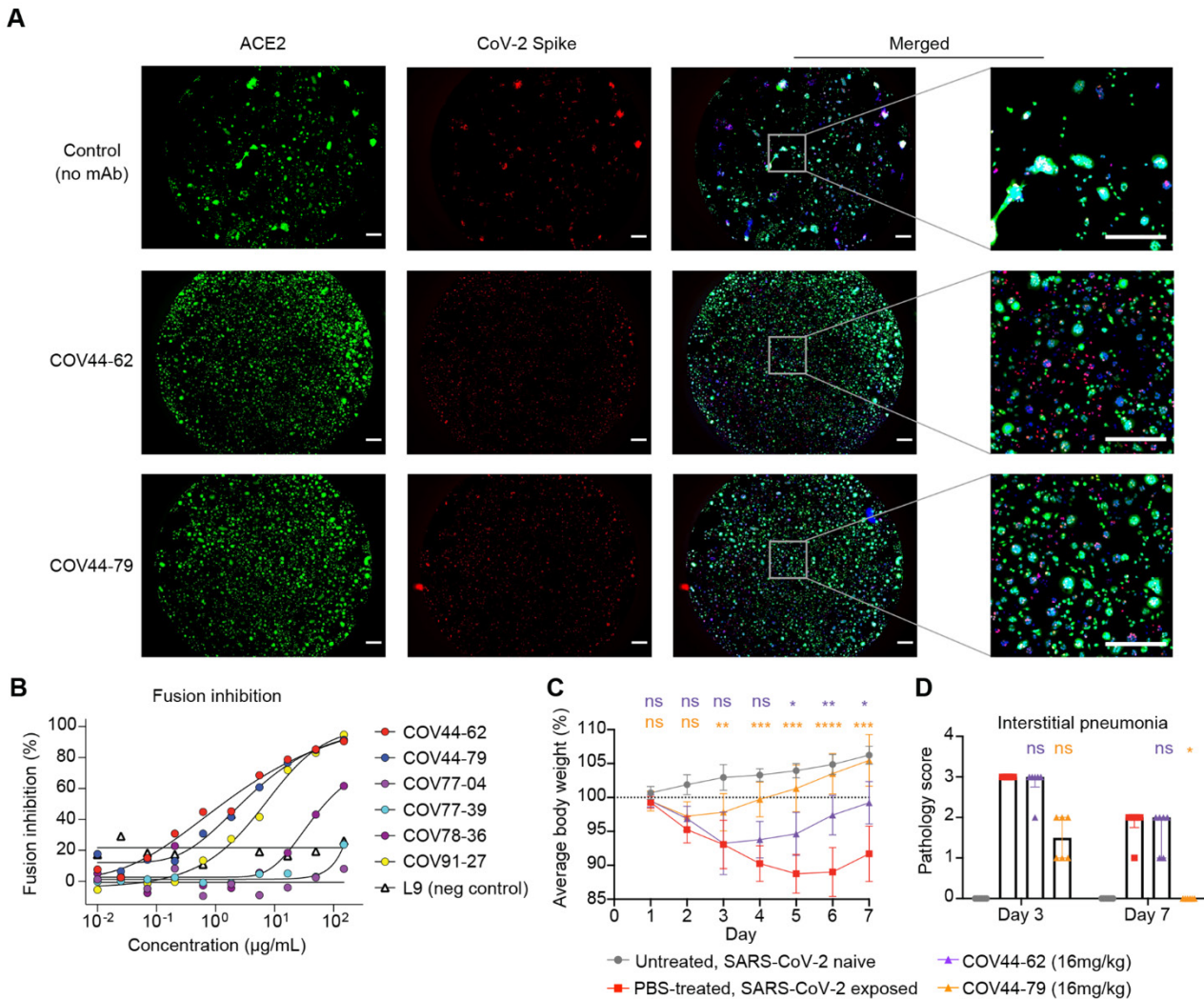


Fig. 5. COV44-62 and COV44-79 inhibit SARS-CoV-2 spike-mediated fusion and COV44-79 limits disease in a Syrian hamster model. (A) Images of fusion between HeLa cells stably expressing SARS-CoV-2 spike (RFP) and HeLa cells stably expressing the ACE2 receptor (GFP) after counter-staining with Hoechst (blue). Cells were co-cultured in the presence of COV44-62, COV44-79 or without a mAb (control). Scale bar, 500 μ m. (B) Fusion inhibition of six fusion peptide-specific mAbs in a quantitative assay. (C) Weight change for SARS-CoV-2 naïve animals versus virus-exposed animals that were mock-treated or treated with 16 mg/kg of mAb. Statistical significance for average body weight was analyzed across the 7-day time-course using a mixed-effects repeated measures model with Dunnett's post-test multiple comparison ($n = 12$ animals from Day 0-3 and $n = 6$ animals from Day 4-7). Error bars show mean \pm SD. (D) Pathology scores for SARS-CoV-2 naïve animals versus virus-exposed animals that were mock-treated or treated with 16 mg/kg of mAb. Scores for interstitial pneumonia pathology (Days 3 and 7) based on gross pathology observations were statistically analyzed by a Kruskal-Wallis test with Dunn's post-test multiple comparison ($n = 6-12$ animals per condition), between the mAb-treated and mock-treated groups on each day. * $P < 0.05$, ** $P < 0.01$, *** $P < 0.001$, **** $P < 0.0001$ and ns, not significant. Bars show median + interquartile range.